Four-body singlet potential-energy surface for reactions of calcium monofluoride

Dibyendu Sardar,[1] Arthur Christianen,[2,3] Hui Li,[1] and John L. Bohn[1,*]

[1]*JILA, NIST, and Department of Physics, University of Colorado, Boulder, Colorado 80309, USA*

[2]*Max-Planck-Institut für Quantenoptik, Hans-Kopfermann-Strasse 1, D-85748 Garching, Germany*

[3]*Munich Center for Quantum Science and Technology, Schellingstraße 4, D-80799 Munich, Germany*

(Received 3 November 2022; accepted 13 March 2023; published 24 March 2023)

A full six-dimensional Born-Oppenheimer singlet potential-energy surface is constructed for the reaction CaF + CaF → CaF_2 + Ca using a multireference configuration-interaction electronic structure calculation. The *ab initio* data thus calculated are interpolated by Gaussian process regression. The four-body potential-energy surface features one D_{2h} global minimum and one C_s local minimum, connected by a barrierless transition state that lends insight to the reaction mechanism. This surface is intended to be of use in understanding ultracold chemistry of CaF molecules.

DOI: 10.1103/PhysRevA.107.032822

I. INTRODUCTION

A recurring goal in the science of ultracold molecules is the possibility to control their chemical reactions, by exploiting control over both internal and motional degrees of freedom. The alkali-metal dimer KRb was an early workhorse in this effort. Its reaction rates have been controlled by temperature [1,2], quantum statistics [3], electric fields [4–8], and optical lattices [9,10]. Moreover, a complete survey of the reaction products K_2 and Rb_2, including their branching ratios, has been performed [11–13]. The lifetime of the collision complex that separates reactants and products in the KRb system has also been measured [14].

Beyond this, a host of experiments involving ultracold alkali-metal dimers have observed anomalously long lifetime of the collision complex, whose origins remain elusive [15–17]. Including these experiments under the general umbrella of ultracold chemistry, this chemistry can be controlled by means of electric field [18,19] or microwave [20] shielding, preventing the molecules from ever getting close enough to react. Such methods have been demonstrated in several laboratories [8,21–23].

The arsenal of molecules that will be available for control of this type is growing rapidly, owing to new advances in laser cooling that allow one to cool and trap even large polyatomic species [24–32]. Among these laser-cooled species, we focus here on the CaF molecule, which has been cooled and trapped in optical tweezers [33–35], raising yet another possibility, that of merging the tweezers and instigating chemical reactions on demand [36]. These molecules are subject to the exothermic reaction

$$\mathrm{CaF} + \mathrm{CaF} \rightarrow \mathrm{CaF_2} + \mathrm{Ca}, \tag{1}$$

releasing approximately 4300 cm^{-1} of energy. The product CaF_2 is widely used in optical applications such as window glass and lenses, although this is of no consequence to the present discussion.

Significantly, this reaction is only possible in the singlet electronic state of the Ca_2F_2 tetramer; the excited triplet state is immune to the reaction. This raises the possibility of controlling the reaction by careful state preparation of the initial spin states of the reactants, a possibility that has been considered in various contexts [12,37–39]. This kind of control could present refined opportunities to, for example, alter branching ratios to the various rovibrational states of the product.

Conceptually, evaluating ultracold chemical reactions splits into considerations of long-range and short-range physics. In the long range, typified by reactants further apart than their van der Waals length, the molecules move slowly and their interactions are given by comparatively weak and well-characterized long-range forces. In this limit, scattering wave functions are comparatively easily calculated. It may be said that propagation from infinity, through this long-range region, can be exploited to prepare the molecules for their entrance into the short-range, chemical cauldron where the reaction takes place.

In this short-range region, forces among the atoms are too strong to be under experimental control, and the native dynamics takes over. This dynamics can be described classically, and therefore ensembles of classical trajectory simulations would illuminate which initial conditions at some transition radius R_0 lead to a desired result—say, emphasizing vibrational excitation of the CaF_2 product over rotations, or vice versa. Control then becomes an issue of solving the long-range quantum-mechanical part of the problem, subject to boundary conditions at R_0 that emphasize flux incident in the desired locations in phase space.

This paper takes the first step in this program by computing a complete *ab initio* short-range singlet potential-energy surface (PES) for the CaF-CaF reaction, to help us better understand the energetics and reaction pathways we may attempt to exploit in the name of control. We note that in the similar context of SrF-SrF cold collisions, a reduced surface

*bohn@murphy.colorado.edu

was proposed some years ago [40]. This reference identified a "handoff" mechanism, whereby one of the F atoms could find itself in a double-well potential in the no-man's land between the alkaline-earth atoms; from here the F could go either way, either completing the reaction or remaining with its initial partner. The calculation of Ref. [40] was limited to a one-dimensional investigation, however.

We construct a full six-dimensional singlet PES for the Ca_2F_2 dimer. We identify global and local minima in this PES, as well as a reaction path that takes the system between them via a submerged barrier. Based on the minimum-energy pathway, we propose a plausible reaction path through which the reaction proceeds by a torsional movement, presenting a richer dynamics than the handoff mechanism of Ref. [40]. A key feature that makes the characterization of this complicated surface possible is that the *ab initio* points, obtained from a MOLPRO calculation, can be readily interpolated using Gaussian process (GP) interpolation, a technique pioneered in this context by Krems and coworkers [41–43].

The presentation of the paper is as follows. In Sec. II, we describe the *ab initio* calculation on the diatomic, triatomic, and tetratomic molecular systems. In Sec. III, we discuss some fundamental features of the GP interpolation including the symmetrization criteria of the Ca_2F_2 surface. The construction of the minimum-energy path and a plausible reaction mechanism of the Ca_2F_2 surface are discussed in Sec. IV. Finally, we make some conclusions in Sec. V.

II. *AB INITIO* CALCULATIONS

In this section, we will describe the *ab initio* calculations of CaF-CaF from the reactant side and CaF_2-Ca from the product side for the concerned reaction: $CaF + CaF \rightarrow CaF_2 + Ca$.

For each arrangement of nuclei in a grid to be described below, an electronic structure calculation is performed using the MOLPRO 2012.1 software package [44]. The electronic configurations of ground-state Ca and F atoms are expressed as $[Ar]4s^2$ and $[He]2s^2 2p^5$, respectively. Thus for the *ab initio* calculations we perform a complete active space self-consistent field calculation (CASSCF) comprising the atomic orbitals $4s$ of Ca and $2p$ of F in the active space. The $3s$ and $3p$ of Ca, as well as the $1s$ and $2s$ of F, were frozen at the Hartree-Fock (HF) level of theory. Thereafter, we carry out an internally contracted multireference configuration-interaction (MRCI) step where single and double excitations are taken relative to this CASSCF reference function where only the $1s$ electrons of F were not correlated. The MRCI calculation incorporates an additional Davidson correction that approximately accounts for the size consistency and higher excitations.

The basis set for Ca is Peterson's pseudopotential-based correlation consistent polarized weighted core valence triple-ζ basis set (cc-pwCVTZ-PP) [45], where the inner core electrons are described by the Stuttgart-Koeln effective core potential (ECP10MDF) [46]. For the F atom, we consider the correlation consistent polarized valence triple basis set (aug-cc-PVTZ) [47] with diffuse augmenting functions. While the method just described is used in constructing the final potential-energy surface, nevertheless at various stages we vary the approach to test its adequacy, as we will see in the following subsections.

A. Diatomic and triatomic molecules

To assess the adequacy of the basis set and method, we first apply them to the three possible diatomic molecules, as well as the product CaF_2. In Table I we make a comparative study of the CaF, Ca_2, and F_2 molecules in terms of the equilibrium bond length (r_e) and depth of the well (D_e), comparing these with previous theoretical and experimental values. In our current method of calculation, the bond length for each of the diatomic molecules agrees with that of literature reported theoretical and experimental value with an error less than 1% which, following common practice in the field, we accept as adequate. With regard to the well depth D_e, our calculations differ from other results by amounts less than $\approx$1000 cm^{-1}, We therefore take this as an estimate of the uncertainty of the calculations. Note that the largest uncertainty belongs to the F_2 molecule.

Similarly, we investigate the global minimum of the potential-energy surface of the CaF_2 product, as summarized in Table II. This table compares the equilibrium bond lengths and bond angle for the ground singlet state of CaF_2 to various values found in the literature. As for the diatomic molecules, we find agreement of the bond lengths below the percent level. The bond angle in CaF_2 remains a matter of some controversy. In various theoretical studies on calcium difluoride [54–59], the ground state is found to be either linear or slightly bent, depending on the quality and size of the basis sets used. The difference in energy between its linear and bent geometry is typically of order tens of cm^{-1}, making the ultimate determination uncertain at present. In our own calculation, the minimum at 168° is separated from the linear geometry by a barrier of only 6 cm^{-1}, meaning our calculation is unlikely to resolve this controversy.

B. Four-body surface

Since CaF is an open-shell molecule having electronic spin 1/2, its dimer either can be a spin singlet ($S = 0$) or a spin triplet state ($S = 1$). In the present calculation, we focus exclusively on the singlet surface as it is the reactive one.

The electronic structure calculations are performed on a grid of relative atoms coordinates. For later interpolation it will be useful if these are roughly equidistant in the parameter space. For this purpose it is useful to consider the coordinate systems which describe well the two asymptotic arrangements of the reactant and product. We choose two suitable coordinate systems to describe the arrangement of atoms for the reactant and product side. We use Jacobi coordinates for the CaF-CaF arrangement as shown in Fig. 1(a), where R_J is the distance between two centers of mass of two monomer CaF molecules having bond lengths r_{13} and r_{24}, respectively. The molecules are tilted with respect to the intermolecular axis by polar angles θ_1 and θ_2, while ϕ_1 is the torsion angle. For the product side (CaF_2-Ca) we use spherical polar coordinates, as depicted in Fig. 1(b). Here, R_c is the distance between two Ca atoms. The bond lengths r_{13} and r_{14} represent the distance between the atoms Ca1-F3 and Ca1-F4. The parameter α is the angle

TABLE I. The comparison of optimized diatom bond lengths r_e in bohrs and depth of the wells D_e in cm^{-1} with previous theoretical and experimental data.

	CaF		Ca_2		F_2	
	r_e	D_e	r_e	D_e	r_e	D_e
This paper	3.704	43672	8.101	1134	2.671	12464
Theory	3.691 [48]	44203 [48]	8.085 [49]	1102 [49]	2.665 [40]	12880 [40]
Expt.	3.717 [50]		8.090 [51]	1075 [51] ±150	2.677 [52]	13410 [53]

between the atoms F3-Ca1-F4, and θ and ϕ_2 are the azimuthal and polar angles, respectively.

Initially, we calculate the optimized geometries of the four-body surface incorporating the basis set described above. Using the method of geometry optimization in MOLPRO [44], we find one global minimum and one local minimum of the four-body surface Ca_2F_2. At present, we are unaware of literature values of either global or local minima of the Ca_2F_2 surface. Therefore, to estimate the uncertainty in our current method of calculation, we determine the same optimization for the global and local minima by another level of theory, coupled-cluster singles, doubles, and perturbative triples excitation [CCSD(T)] using the same basis sets: Ca = cc-pwCVTZ-PP and F = aug-cc-PVTZ. For both of the minima, the geometric parameters and corresponding energies are tabulated in Table III for both *ab initio* methods.

Both calculations confirm that the global minimum of the Ca_2F_2 surface has a D_{2h} symmetry with a rhombic structure for which the bond lengths satisfy $r_{13} = r_{24} = r_{23} = r_{14}$, and that the local minimum has C_s symmetry. The two calculations moreover agree on the bond lengths at the usual percent level of accuracy.

The energies of these minima, however, differ by up to ≈1000 cm^{-1}, with the CCSD(T) calculation consistently finding deeper minima. It may be presumed that the CCSD(T) calculation is more accurate, because it includes higher-order electronic correlations. However, CCSD(T) is not generally well behaved across a reaction pathway, and therefore using CCSD(T) for the entire PES will expectedly lead to irregularities. We therefore chose to carry out the calculations on the MRCI level. In this context, we therefore use the results of Table III to estimate the uncertainty of our calculation as on the order of ≈1000 cm^{-1}, consistent in fact with the diatomic molecule calculations.

Finally, we check the quality of our chosen basis set for Ca which is used throughout our *ab initio* calculation. The comparison of the global well depth in our standard cc-pwCVTZ-PP basis set for Ca is compared to three other basis sets with longer acronyms in Table IV. The basis set aug-cc-PVTZ is assumed for F throughout. The difference so induced is seen to be of order ≈100 cm^{-1}, whereby the influence of the Ca basis set is not regarded as a significant source of uncertainty.

Thus encouraged that the electronic structure calculations are sound, we proceed to use the MRCI method with the basis sets described above, to calculate the four-body potential-energy surface. Focusing here on the short-range part of the surface relevant to the chemical reaction, we limit the range of atomic coordinates as follows: For the CaF-CaF reactant arrangement, we consider coordinates bounded by (1) monomer bond lengths of CaF (r_{13}, r_{24}) varying from $3.2a_0$ to $7a_0$ with $r_{24} > r_{13}$ and (2) R_J varying from $4.0a_0$ to $18a_0$; the angles θ_1, θ_2, and ϕ_1 vary from zero to π. The corresponding range of product coordinates is given by (1) $3.3a_0 < r_{13} < 7a_0$, (2) $3.4a_0 < r_{14} < 7.2a_0$, (3) $4a_0 < R_c < 15a_0$, and (4) $0 < \alpha, \theta, \phi_2 < \pi$.

TABLE II. Optimized molecular parameters of calcium difluoride where bond lengths (r_1 and r_2) are in bohrs and bond angle β is in degrees.

	Symmetry	r_1	r_2	β
This paper	$^1A_1$	3.804	3.804	168.10
Theory [58]	$^1A_1$	3.799	3.799	157.50
Theory [59]	$^1A_1$	3.790	3.790	154.86

III. MACHINE-LEARNING ALGORITHM: GAUSSIAN PROCESS REGRESSION

Traditionally, interpolation of potential-energy surfaces was an art form that required careful assessment of the appropriate fitting functions in various regions of configuration space, followed by accurate determination of the parameters of these fitting functions. This situation has changed recently with the use of GP interpolation methods, pioneered in this context by Cui and Krems [60]. In these methods, the computed *ab initio* values of the PES at a set of atom coordinates allow a direct estimate of the value of the PES at a new point at which the *ab initio* calculation was not performed.

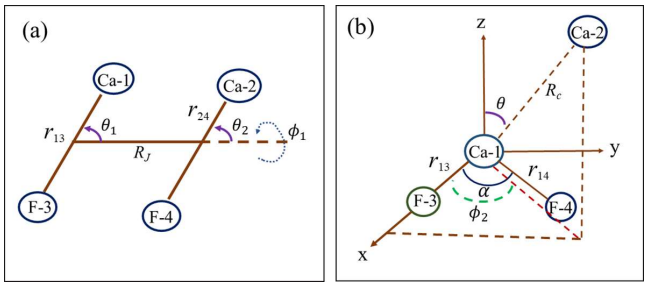

FIG. 1. (a) The Jacobi coordinates of the complex in one of the CaF-CaF arrangements. (b) The spherical polar coordinates for one of the arrangements of CaF_2-Ca.

TABLE III. The energy of the PES Ca_2F_2 in cm^{-1} for the global and local minima with optimized bond lengths (in bohrs). The energies are referred to the CaF + CaF dissociation threshold.

Method	Geometry	r_{12}	r_{13}	r_{34}	r_{23}	r_{24}	r_{14}	E_{min}
CCSD(T)	D_{2h}	6.360	4.057	5.039				−18923
MRCI		6.401	4.053	4.979				−17936
CCSD(T)	C_s	6.522	3.756	7.337	4.076	4.007	10.268	−15363
MRCI		6.606	3.743	7.327	4.064	4.006	10.337	−14924

This process proceeds directly without the intermediate step of determining a fitting function. For the final potential-energy surface in the GP fitting we use inverse atomic distance coordinates. Because it is difficult to describe different chemical arrangements of the four-body system equivalently by Jacobi coordinates, making it troublesome to fit the reactive part of the PES [41], we choose inverse interatomic spacing coordinates.

Let $\mathbf{x}$ denote a set of six coordinates that defines a configuration of atoms (e.g., these are the inverse interatomic spacings in the coordinate system we use). There is presumed to exist a continuous PES in these coordinates, denoted $V(\mathbf{x})$. The *ab initio* calculation provides a discrete set of such values, $y_i = V(\mathbf{x}_i)$, referred to as the training set in the machine learning argot. The *possible* values of the PES at the points $\mathbf{x}_i$ are assumed to satisfy some Gaussian-like probability distribution:

$$P(\{V_i\}) \propto \exp\left[-\frac{1}{2}\sum_{ij} y_i K^{-1}(\mathbf{x}_i, \mathbf{x}_j) y_j\right]. \tag{2}$$

Here the function K, called a kernel, describes the covariance of the variables in this distribution. Significantly, the kernel is a function of the values $\mathbf{x}_i$ at which the data are computed, and not of the computed values V_i themselves. The functional form of K is relevant to the quality of the fit. Typically it contains parameters such as a characteristic length scale, so that, for example, the data at two points $\mathbf{x}_i$ and $\mathbf{x}_j$ are correlated only if $|\mathbf{x}_i - \mathbf{x}_j|$ is smaller than this scale. Thus the kernel can describe features like the smoothness of the fit, but without specifying a particular fitting function.

In the interpolation step, it is desired to know the predicted value y^* of the PES at a new configuration $\mathbf{x}^*$ at which the *ab initio* calculation has not been performed. To make this interpolation, it is assumed that the additional point would satisfy the same distribution with a kernel of the same functional form. In this case a standard algebraic manipulation yields a distribution for the unknown value y^*, with mean value and standard deviation [61]:

$$\mu(\mathbf{x}_*) = K(\mathbf{x}_*, \mathbf{x})^T \left[K(\mathbf{x}, \mathbf{x}) + \sigma_n^2 I\right]^{-1} \mathbf{y}, \tag{3}$$

$$\sigma(\mathbf{x}_*) = K(\mathbf{x}_*, \mathbf{x}_*) - K(\mathbf{x}_*, \mathbf{x})^T \left[K\left(\mathbf{x}, \mathbf{x} + \sigma_n^2 I\right)\right]^{-1} K(\mathbf{x}_*, \mathbf{x}). \tag{4}$$

There are many functional forms possible for the kernel function. For each such case, the kernel depends on some set of parameters, which are optimized by maximizing the log marginal likelihood:

$$\ln p(\mathbf{y}|\mathbf{x}; \theta_3) = -\tfrac{1}{2}\mathbf{y}^T K^{-1}\mathbf{y} - \tfrac{1}{2}\ln|K| - \tfrac{n}{2}\ln(2\pi) \tag{5}$$

where $|K|$ is the determinant of K and θ_3 denotes the collective set of parameters for the analytical function of $\mathbb{k}$ (see below).

The optimum quality of GP fit for a multidimensional surface depends on the kernel and the coordinate representation. Here, we consider inverse atomic distance coordinates for GP fitting. Following the GP fits of potential-energy surfaces in Ref. [41], the kernel we use is the product of a Matérn kernel [61] and constant kernel [61]. This kernel takes the form

$$\mathbb{k}(\mathbf{x}_i, \mathbf{x}_j) = CM(\mathbf{x}_i, \mathbf{x}_j, l_1, l_2, l_3, l_4, l_5, l_6) \tag{6}$$

where C is the constant kernel. Here, M is the anisotropic Matérn kernel depending on the parameter (ν) besides length scales [61]. For $\nu = 2.5$, the Matérn kernel is defined as [41,61]

$$M(\mathbf{x}_i, \mathbf{x}_j) = \sum_{k=1}^{6}\left[1 + \sqrt{5}l_k^{-1}|x_{i,k} - x_{j,k}| + \frac{5}{3}l_k^{-2}|x_{i,k} - x_{j,k}|^2\right] \times \exp\left(-\sqrt{5}l_k^{-2}|x_{i,k} - x_{j,k}|^2\right). \tag{7}$$

The characteristic length scales $l_1 - l_6$ are the parameters of θ_3.

In general, validity of the GP model increases monotonically with an increase in the number of training points. However, for evaluating the PES with n training points, GP involves an iterative inversion of a square matrix $n \times n$, scaling as $O(n^3)$. But, numerical evaluation of a GP model can be reduced to a product of two vectors of size n, scaling as $O(n)$. Therefore, one needs to care about n so that the maximum number of training points should lie in the configuration space. Besides this, insertion of the symmetrization in the GP model is essential to explore the reactive part of the surface entirely since GP has no prior information about the symmetry.

TABLE IV. The comparison of well depth (D_e) in cm^{-1} with different basis sets of Ca for the global minimum of Ca_2F_2.

Serial no.	Basis	Depth of well (D_e)	Error (%)
1	cc-pwCVTZ-PP	17936	
2	cc-pCVQZ-PP [45]	17787	0.83
3	cc-pwCVQZ-PP [45]	17885	0.29
4	aug-cc-pwCVQZ-PP [45]	17927	0.05

A. Symmetrization of GP

The PES as interpolated by the Gaussian process must be symmetric under the exchange of either the two Ca nuclei, or the two F nuclei. Accounting for this symmetry can reduce the configuration space over which the fit must be performed. Besides, we add some symmetrically equivalent points to the training set to improve the quality around the symmetrization boundaries. Let us define the permutation operators $\hat{P}_{12}$ that interchange the Ca nuclei and $\hat{P}_{34}$ that exchange the F nuclei. Then the permutation operators $\hat{P}_{12}$, $\hat{P}_{34}$, and $\hat{P}_{12}\hat{P}_{34}$ give equivalent energy when two nuclei permute. For the CaF-CaF arrangement, we consider the training point region

where $r_{13} < r_{24}$ and that also fulfills $(r_{13} + r_{24}) < (r_{14} + r_{23})$ since r_{13} and r_{24} are the bond lengths of each CaF monomer in the chosen Jacobi coordinate. In the spherical polar coordinates of $CaF_2 + Ca$ arrangement, the training points region is considered where $r_{13} < r_{14}$.

In our GP model, the symmetrization procedure is accomplished by coupling different contributions utilizing a switching function. Supposing we consider two functions $F_1(\vec{x})$ and $F_2(\vec{x})$ between which the switch is made, then

$$F_m[u; m, w, F_1(\vec{x}), F_2(\vec{x})] = z(u, c, w)F_1(\vec{x}) + [1 - z(u, c, w)]F_2(\vec{x}) \quad (8)$$

where the sigmoid function z should be twice differentiable and switches within the finite interval $(c - w) < u < (c + w)$, and it can be expressed as [41]

$$z(u, c, w) = \begin{cases} 0, & \text{if } u \leqslant c - w \\ \frac{1}{2} + \frac{9}{16}\sin\frac{\pi(u-c)}{2w} + \frac{1}{16}\sin\frac{3\pi(u-c)}{2w}, & \text{if } c - w < u < c + w \\ 1, & \text{if } u \geqslant c + w \end{cases}.$$

Here, u is the parametrizing parameter for switching, c is the value of u around which the switch is centered, and w is the half width of the switching interval. The symmetrization scheme for the CaF-CaF region is given as

$$V_1^{\mathrm{GP}}(\vec{x}) = F_m\left[\frac{r_{13}}{r_{13} + r_{24}}; \frac{1}{2}, \frac{1}{16}, V^{\mathrm{GP}}(\vec{x}), V^{\mathrm{GP}}(\hat{P}_{12}\hat{P}_{34}\vec{x})\right], \quad (9)$$

$$V_2^{\mathrm{GP}}(\vec{x}) = F_m\left[\frac{r_{23}}{r_{23} + r_{14}}; \frac{1}{2}, \frac{1}{16}, V^{\mathrm{GP}}(\hat{P}_{12}\vec{x}), V^{\mathrm{GP}}(\hat{P}_{34}\vec{x})\right], \quad (10)$$

$$V_{\mathrm{CaF\text{-}CaF}}^{\mathrm{GP}}(\vec{x}) = F_m\left[\frac{r_{13} + r_{24}}{r_{13} + r_{24} + r_{23} + r_{14}}; \frac{1}{2}, \frac{1}{16}, V_1^{\mathrm{GP}}(\vec{x}), \times V_2^{\mathrm{GP}}(\vec{x})\right]. \quad (11)$$

For the CaF_2-Ca region,

$$V_3^{\mathrm{GP}}(\vec{x}) = F_m\left[\frac{r_{13}}{r_{13} + r_{14}}; \frac{1}{2}, \frac{1}{16}, V^{\mathrm{GP}}(\vec{x}), V^{\mathrm{GP}}(\hat{P}_{34}\vec{x})\right], \quad (12)$$

$$V_4^{\mathrm{GP}}(\vec{x}) = F_m\left[\frac{r_{23}}{r_{23} + r_{24}}; \frac{1}{2}, \frac{1}{16}, V^{\mathrm{GP}}(\hat{P}_{12}\vec{x}), V^{\mathrm{GP}}(\hat{P}_{12}\hat{P}_{34}\vec{x})\right], \quad (13)$$

$$V_{\mathrm{CaF_2\text{-}Ca}}^{\mathrm{GP}}(\vec{x}) = F_m\left[\frac{r_{13} + r_{14}}{r_{13} + r_{14} + r_{23} + r_{24}}; \frac{1}{2}, \frac{1}{16}, V_3^{\mathrm{GP}}(\vec{x}), \times V_4^{\mathrm{GP}}(\vec{x})\right]. \quad (14)$$

Finally we merge the above two arrangements as

$$V_{12}^{\mathrm{GP}}(\vec{x}) = F_m\left[\frac{r_{24}}{r_{14} + r_{24}}; \frac{1}{2}, \frac{1}{16}, V_1^{\mathrm{GP}}(\vec{x}), V_3^{\mathrm{GP}}(\vec{x})\right], \quad (15)$$

$$V_{34}^{\mathrm{GP}}(\vec{x}) = F_m\left[\frac{r_{14}}{r_{14} + r_{24}}; \frac{1}{2}, \frac{1}{16}, V_2^{\mathrm{GP}}(\vec{x}), V_4^{\mathrm{GP}}(\vec{x})\right], \quad (16)$$

$$V_{\mathrm{total}}^{\mathrm{GP}}(\vec{x}) = F_m\left[\frac{r_{13}}{r_{13} + r_{23}}; \frac{1}{2}, \frac{1}{16}, V_{12}^{\mathrm{GP}}(\vec{x}), V_{34}^{\mathrm{GP}}(\vec{x})\right]. \quad (17)$$

B. Interpolation of the surface by GP models

For the construction of the GP model, the *ab initio* energies are calculated on selected grids, respecting the symmetrization as described above. The grid points are chosen within the range of Jacobi and spherical coordinates as described above, and based on a sampling method developed in Ref. [41]. In this method, we initially perform the HF calculations on a random but roughly equidistant grid using the method of latin hypercube sampling [62]. We reject grid points where the energy of the PES is above a cutoff energy, as being both irrelevant to the surface, and problematic to interpolate. The selection of the cutoff energy in different regions in the parameter space is considered in the following way: If any of the interparticle distances between Ca and F is smaller than $3.4a_0$ and if $R < 10a_0$, then we use a cutoff of 5000 cm^{-1}. If one of these two criteria is false we use a lower value of the cutoff, given by 1000 cm^{-1}. This procedure is chosen so that a proper repulsive barrier is included in the short range without wasting training points to describe the vibrational potential of the free diatoms in the long range. At the points that remain, we construct the training set using the full MRCI algorithm described above using inverse atomic distance coordinates.

To test the accuracy of the GP interpolation, we optimize the global and local minima of the PES Ca_2F_2 for two distinct sets of training points, referring to the resulting fits as GP-I and GP-II. These two sets consist of 2596 and 3061 training points, respectively. We use the steepest gradient descent approach for optimization. As reported in Table V, the optimized energies of the two minima agree within ≈500 cm^{-1} with the *ab initio* calculation, for both GP fits. The error is comparable to the uncertainty in the electronic structure cal-

TABLE V. The energy of the PES Ca_2F_2 in cm^{-1} for the global and local minima with optimized bond lengths (in bohrs).

Method	Geometry	r_{12}	r_{13}	r_{34}	r_{23}	r_{24}	r_{14}	E_{min}
GP-I	D_{2h}	6.355	4.085	5.136				−18417
GP-II		6.400	4.043	4.958				−17847
GP-I	C_s	6.320	3.678	7.046	4.176	4.140	9.942	−14907
GP-II		6.323	3.648	6.994	4.336	4.058	9.900	−14330

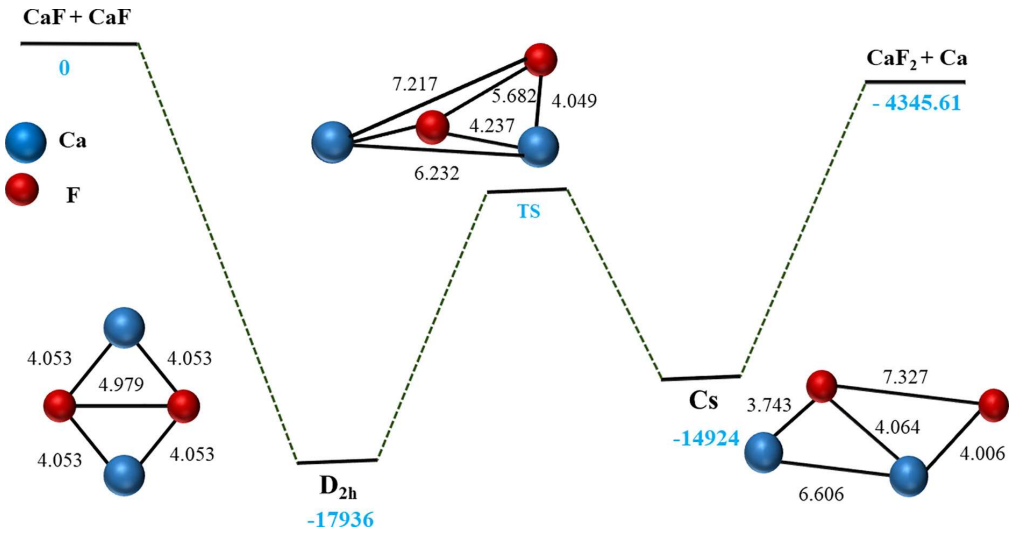

FIG. 2. A reaction pathway for the reaction CaF + CaF → CaF_2 + Ca with energies and geometries of the stationary points. The red and blue balls indicate the atoms Ca and F, respectively. The distance between two atoms is in bohrs. The energies are in cm^{-1} with respect to the CaF-CaF threshold.

culations. This suggests that the number of training points is adequate.

As a second check, an additional set of test points is extracted from the *ab initio* electronic structure calculation. We can then compare these directly to the values approximated from the GP fit, and determine the root-mean-squared error in the fit of the test points. This error is on the order of 1200 cm^{-1} for 1330 randomly chosen test points, another confirmation of the accuracy of the fit.

Based on the result including the *ab initio* method of calculation, we find uncertainties on the order of ≈1000 cm^{-1} for the electronic structure calculation, and ≈1200 cm^{-1} for the GP fit. Therefore, assuming these uncertainties are independent, we estimate the net uncertainty to be perhaps ≈1500 cm^{-1}, or something like 8% of the depth of the potential. The training set GP-II is made available online at GitHub [63], along with the fitting routine. In addition, a larger set, GP-III, is also available for exploration.

IV. MINIMUM-ENERGY PATH

The complete potential-energy surface is therefore ready for dynamical calculations to begin, a task we defer to a future work. However, an overview of the surface is warranted here, as a first hint of the reaction mechanism. To this end we sketch the reaction path shown in Fig. 2. The first thing to note is that the reaction CaF + CaF → CaF_2 +F is exothermic, releasing 4300 cm^{-1} of energy.

To get from reactants to products, we trace a hypothetical minimum-energy path, described by the way stations illustrated in Fig. 3. Some of the evolving geometries along this path are indicated by letters (a)–(g) and are being analyzed later. This diagram includes the global minimum of D_{2h} symmetry and the local minimum of C_s symmetry, as identified above. In between there exists a saddle point, with geometry and energy as shown, and which we identify in this context as a transition state. Significantly, the energy of this state is well below the reactant and product energies, whereby the transition state occurs via a submerged barrier.

The transition state is identified using the "climbing image nudged elastic band" [64] approach. In this method, a set of intermediate states (15 in this case) is posited between the two minima. These points are treated conceptually as point masses, called "beads," subject to the energy constraint of the PES itself, and to imaginary spring forces artificially applied between each bead and the next. The minimum-energy path between the potential minima is then obtained by minimizing the energy of this system of masses. This method produces the energy diagram in Fig. 3, constructed using the GP-II interpolation described above. This figure shows how the energy rises and falls in going between the D_{2h} minimum on the left, and the C_s minimum on the right. The blue spheres represent the locations of the beads along this trajectory, and the energies at the corresponding points of the PES. The highest-energy state along this line is therefore associated with the transition state. The red curve is an interpolation to guide the eye.

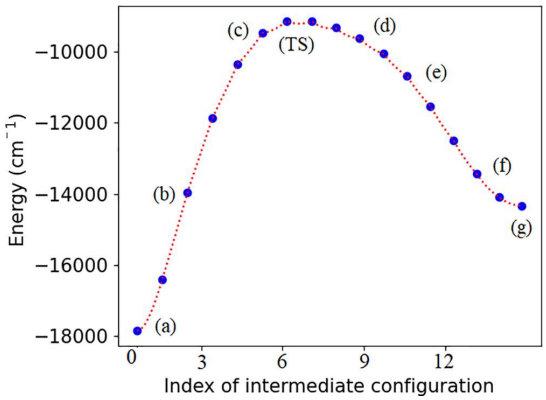

FIG. 3. A transition path between D_{2h} and C_s minima of the Ca_2F_2 potential surface. The letters (a)–(g) represent the evolution of the geometries along the minimum-energy path.

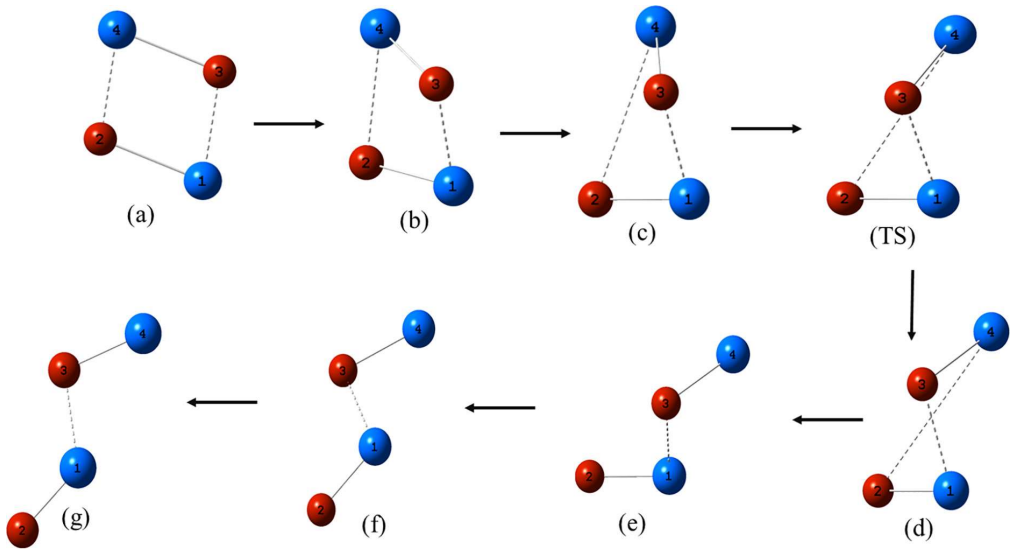

FIG. 4. The evolution of the geometries on passing from global minimum (a) to local minimum (g) along the minimum-energy path involving the transition state (TS). Blue spheres represent Ca atoms, while red spheres represent F atoms.

Figure 4 illustrates the atomic configurations at various steps along this trajectory. One presumes these are given in order as the reaction coordinate grows from small to large; one of them is the transition state. The geometric parameters of the TS are $r_{12} = 6.232$, $r_{13} = 3.866$, $r_{23} = 4.237$, $r_{14} = 7.217$, $r_{24} = 4.049$, and $r_{34} = 5.682$, in bohrs. We note that the geometry of the transition state is not linear. In these drawings the blue circles represent Ca atoms, and the red circles represent F atoms.

The main result shows the evolution in geometry is to move the atoms from the D_{2h} symmetry in Fig. 4(a), to the zig-zag formation in Fig. 4(g). From this point, the lower calcium atom has two fluorine neighbors, which it is ready to take away as the CaF_2 product. To get between these arrangements, the F atom in the upper right of Fig. 4(a) swings around, out of the plane of the figure, thereby moving from right to left. Thus, at least along the reaction path shown, the reaction proceeds by a torsional movement, suggesting that the product may be put into significant rotation. Also since the lower F atom remains more or less a spectator to the process, it might be expected that its CaF bond receives less energy than the other bond, leading to asymmetric stretch modes of the product.

Contrast this with the simple handoff mechanism of Ref. [40], explored in the very similar reaction of SrF + SrF. Restricted to a single spatial coordinate, the F atom in that model was constrained to move in the space between two Sr atoms, and to choose one or another during the collision event. Inasmuch as this was the only allowed degree of freedom, it could be expected that the SrF stretch motion would be excited in the F extraction reaction, but no rotation. In contrast, the present result shows clearly that, along the minimum-energy path, the F atom to be transferred swings around the line joining the Ca atoms, thus imputing a likely rotation of this bond. In context, this discovery is significant: we now expect that both rotations and vibrations are easily capable of excitation during the reaction. There is therefore a clear branching ratio to attempt to control, namely, that between vibrationally excited and rotationally excited products.

These conclusions remain, of course, speculative at this point, and will have to be assessed in dynamical calculations. In particular, following these configurations along an adiabatic path such as this one completely disregards the influence of the energy the reactants actually have, as they commence the reaction approximately 18 000 cm^{-1} above the global minimum. Nevertheless, even in this approximation, it can be seen that a nontrivial rearrangement may occur, leading to interesting rovibrational branching ratios, which may ultimately be the subject of control in the ultracold environment.

V. CONCLUSION

In summary, we have constructed a six-dimensional singlet potential-energy surface of the Ca_2F_2 system at short range and analyzed the features and reactivity of the surface. We observed the reaction CaF + CaF → CaF_2 +Ca is exothermic in nature by liberating energy ≈4300 cm^{-1}. The complete construction of the Ca_2F_2 surface depends on two steps. First the *ab initio* points were calculated using the multireference configuration-interaction method in MOLPRO and then these points were readily interpolated by GP fitting. We detected one global minimum and one local minimum having D_{2h} and C_s symmetry, respectively, and we constructed a minimum-energy path between these two minima that connects them via a submerged barrier. We proposed a plausible reaction pathway for the formation of the products. However, one can perform a dynamic calculation to establish the true reaction mechanism for the singlet reactive surface CaF-CaF which is beyond the scope of our paper. We hope this PES will provide an initial platform to study the dynamics of the reaction.

In future work, we will explore both the triplet surface and spin-orbit coupling to the reactive singlet surface. The triplet surface is nonreactive and suppresses the chemical reaction.

Therefore, if we presume a model where initially the sample is prepared in the spin-polarized triplet state and thereafter switches on the spin-orbit coupling to the singlet surface, we anticipate the reactivity of the singlet surface where the coupling parameter is significant between these two surfaces, resulting in a chemical reaction. Therefore, the conversion of the spin-polarized nonreactive surface to the non-spin-polarized reactive state can be studied including the branching ratios. This could impart a new direction in the domain of controlled chemical reactions.

ACKNOWLEDGMENTS

This material is based upon work supported by NSF Grant No. PHY 1734006. We also acknowledge funding from AFOSR–Multidisciplinary University Research Initiatives Grant No. GG016303. D.S. especially acknowledges discussions with Kirk A. Peterson and Tijs Karman for *ab initio* calculations, and we are thankful to Roman V. Krems, Jacek Kłos, Timur Tscherbul, and Michał Tomza for initial discussions.

[1] S. Ospelkaus, K.-K. Ni, D. Wang, M. De Miranda, B. Neyenhuis, G. Quéméner, P. Julienne, J. Bohn, D. Jin, and J. Ye, Quantum-state controlled chemical reactions of ultracold potassium-rubidium molecules, Science **327**, 853 (2010).

[2] L. De Marco, G. Valtolina, K. Matsuda, W. G. Tobias, J. P. Covey, and J. Ye, A degenerate Fermi gas of polar molecules, Science **363**, 853 (2019).

[3] G. Valtolina, K. Matsuda, W. G. Tobias, J.-R. Li, L. De Marco, and J. Ye, Dipolar evaporation of reactive molecules to below the fermi temperature, Nature (London) **588**, 239 (2020).

[4] K.-K. Ni, S. Ospelkaus, D. Wang, G. Quéméner, B. Neyenhuis, M. De Miranda, J. Bohn, J. Ye, and D. Jin, Dipolar collisions of polar molecules in the quantum regime, Nature (London) **464**, 1324 (2010).

[5] G. Quéméner and J. L. Bohn, Strong dependence of ultracold chemical rates on electric dipole moments, Phys. Rev. A **81**, 022702 (2010).

[6] G. Quéméner and J. L. Bohn, Dynamics of ultracold molecules in confined geometry and electric field, Phys. Rev. A **83**, 012705 (2011).

[7] G. Wang and G. Quéméner, Tuning ultracold collisions of excited rotational dipolar molecules, New J. Phys. **17**, 035015 (2015).

[8] K. Matsuda, L. De Marco, J.-R. Li, W. G. Tobias, G. Valtolina, G. Quéméner, and J. Ye, Resonant collisional shielding of reactive molecules using electric fields, Science **370**, 1324 (2020).

[9] M. H. G. de Miranda, A. Chotia, B. Neyenhuis, D. Wang, G. Quéméner, S. Ospelkaus, J. Bohn, J. Ye, and D. Jin, Controlling the quantum stereodynamics of ultracold bimolecular reactions, Nat. Phys. **7**, 502 (2011).

[10] W. G. Tobias, K. Matsuda, J.-R. Li, C. Miller, A. N. Carroll, T. Bilitewski, A. M. Rey, and J. Ye, Reactions between layer-resolved molecules mediated by dipolar spin exchange, Science **375**, 1299 (2022).

[11] M.-G. Hu, Y. Liu, D. D. Grimes, Y.-W. Lin, A. H. Gheorghe, R. Vexiau, N. Bouloufa-Maafa, O. Dulieu, T. Rosenband, and K.-K. Ni, Direct observation of bimolecular reactions of ultracold krb molecules, Science **366**, 1111 (2019).

[12] M.-G. Hu, Y. Liu, M. A. Nichols, L. Zhu, G. Quéméner, O. Dulieu, and K.-K. Ni, Nuclear spin conservation enables state-to-state control of ultracold molecular reactions, Nat. Chem. **13**, 435 (2021).

[13] Y. Liu, M.-G. Hu, M. A. Nichols, D. Yang, D. Xie, H. Guo, and K.-K. Ni, Precision test of statistical dynamics with state-to-state ultracold chemistry, Nature (London) **593**, 379 (2021).

[14] Y. Liu, M.-G. Hu, M. A. Nichols, D. D. Grimes, T. Karman, H. Guo, and K.-K. Ni, Photo-excitation of long-lived transient intermediates in ultracold reactions, Nat. Phys. **16**, 1132 (2020).

[15] P. D. Gregory, J. A. Blackmore, S. L. Bromley, and S. L. Cornish, Loss of Ultracold ^{87}Rb ^{133}Cs Molecules via Optical Excitation of Long-Lived Two-Body Collision Complexes, Phys. Rev. Lett. **124**, 163402 (2020).

[16] R. Bause, A. Schindewolf, R. Tao, M. Duda, X.-Y. Chen, G. Quéméner, T. Karman, A. Christianen, I. Bloch, and X.-Y. Luo, Collisions of ultracold molecules in bright and dark optical dipole traps, Phys. Rev. Res. **3**, 033013 (2021).

[17] P. Gersema, K. K. Voges, M. Meyer zum Alten Borgloh, L. Koch, T. Hartmann, A. Zenesini, S. Ospelkaus, J. Lin, J. He, and D. Wang, Probing Photoinduced Two-Body Loss of Ultracold Nonreactive Bosonic ^{23}Na ^{87}Rb and ^{23}Na ^{39}K Molecules, Phys. Rev. Lett. **127**, 163401 (2021).

[18] G. Quéméner and J. L. Bohn, Shielding $^2\Sigma$ ultracold dipolar molecular collisions with electric fields, Phys. Rev. A **93**, 012704 (2016).

[19] M. L. González-Martínez, J. L. Bohn, and G. Quéméner, Adimensional theory of shielding in ultracold collisions of dipolar rotors, Phys. Rev. A **96**, 032718 (2017).

[20] T. Karman and J. M. Hutson, Microwave Shielding of Ultracold Polar Molecules, Phys. Rev. Lett. **121**, 163401 (2018).

[21] L. Anderegg, S. Burchesky, Y. Bao, S. S. Yu, T. Karman, E. Chae, K.-K. Ni, W. Ketterle, and J. M. Doyle, Observation of microwave shielding of ultracold molecules, Science **373**, 779 (2021).

[22] J.-R. Li, W. G. Tobias, K. Matsuda, C. Miller, G. Valtolina, L. De Marco, R. R. Wang, L. Lassablière, G. Quéméner, J. L. Bohn *et al.*, Tuning of dipolar interactions and evaporative cooling in a three-dimensional molecular quantum gas, Nat. Phys. **17**, 1144 (2021).

[23] A. Schindewolf, R. Bause, X.-Y. Chen, M. Duda, T. Karman, I. Bloch, and X.-Y. Luo, Evaporation of microwave-shielded polar molecules to quantum degeneracy, arXiv:2201.05143.

[24] E. S. Shuman, J. F. Barry, and D. DeMille, Laser cooling of a diatomic molecule, Nature (London) **467**, 820 (2010).

[25] I. Kozyryev, L. Baum, K. Matsuda, B. L. Augenbraun, L. Anderegg, A. P. Sedlack, and J. M. Doyle, Sisyphus Laser Cooling of a Polyatomic Molecule, Phys. Rev. Lett. **118**, 173201 (2017).

[26] L. Anderegg, B. L. Augenbraun, Y. Bao, S. Burchesky, L. W. Cheuk, W. Ketterle, and J. M. Doyle, Laser cooling of optically trapped molecules, Nat. Phys. **14**, 890 (2018).

[27] L. W. Cheuk, L. Anderegg, B. L. Augenbraun, Y. Bao, S. Burchesky, W. Ketterle, and J. M. Doyle, Λ-Enhanced Imaging of Molecules in an Optical Trap, Phys. Rev. Lett. **121**, 083201 (2018).

[28] D. Mitra, N. B. Vilas, C. Hallas, L. Anderegg, B. L. Augenbraun, L. Baum, C. Miller, S. Raval, and J. M. Doyle, Direct laser cooling of a symmetric top molecule, Science **369**, 1366 (2020).

[29] S. Ding, Y. Wu, I. A. Finneran, J. J. Burau, and J. Ye, Sub-doppler Cooling and Compressed Trapping of yo Molecules at μK Temperatures, Phys. Rev. X **10**, 021049 (2020).

[30] B. L. Augenbraun, J. M. Doyle, T. Zelevinsky, and I. Kozyryev, Molecular Asymmetry and Optical Cycling: Laser Cooling Asymmetric Top Molecules, Phys. Rev. X **10**, 031022 (2020).

[31] L. Baum, N. B. Vilas, C. Hallas, B. L. Augenbraun, S. Raval, D. Mitra, and J. M. Doyle, 1D Magneto-Optical Trap of Polyatomic Molecules, Phys. Rev. Lett. **124**, 133201 (2020).

[32] N. B. Vilas, C. Hallas, L. Anderegg, P. Robichaud, A. Winnicki, D. Mitra, and J. M. Doyle, Magneto-optical trapping and sub-doppler cooling of a polyatomic molecule, Nature (London) **606**, 70 (2022).

[33] V. Zhelyazkova, A. Cournol, T. E. Wall, A. Matsushima, J. J. Hudson, E. A. Hinds, M. R. Tarbutt, and B. E. Sauer, Laser cooling and slowing of caf molecules, Phys. Rev. A **89**, 053416 (2014).

[34] S. Truppe, H. Williams, M. Hambach, L. Caldwell, N. Fitch, E. Hinds, B. Sauer, and M. Tarbutt, Molecules cooled below the doppler limit, Nat. Phys. **13**, 1173 (2017).

[35] L. Anderegg, L. W. Cheuk, Y. Bao, S. Burchesky, W. Ketterle, K.-K. Ni, and J. M. Doyle, An optical tweezer array of ultracold molecules, Science **365**, 1156 (2019).

[36] L. W. Cheuk, L. Anderegg, Y. Bao, S. Burchesky, S. S. Yu, W. Ketterle, K.-K. Ni, and J. M. Doyle, Observation of Collisions between Two Ultracold Ground-State CaF Molecules, Phys. Rev. Lett. **125**, 043401 (2020).

[37] T. Sikorsky, Z. Meir, R. Ben-Shlomi, N. Akerman, and R. Ozeri, Spin-controlled atom–ion chemistry, Nat. Commun. **9**, 1 (2018).

[38] A. Mohammadi, A. Krükow, A. Mahdian, M. Deiß, J. Pérez-Ríos, H. da Silva, M. Raoult, O. Dulieu, and J. Hecker Denschlag, Life and death of a cold barb$^+$ molecule inside an ultracold cloud of rb atoms, Phys. Rev. Res. **3**, 013196 (2021).

[39] H. Son, J. J. Park, Y.-K. Lu, A. O. Jamison, T. Karman, and W. Ketterle, Control of reactive collisions by quantum interference, Science **375**, 1006 (2022).

[40] E. R. Meyer and J. L. Bohn, Chemical pathways in ultracold reactions of srf molecules, Phys. Rev. A **83**, 032714 (2011).

[41] A. Christianen, T. Karman, R. A. Vargas-Hernández, G. C. Groenenboom, and R. V. Krems, Six-dimensional potential energy surface for nak–nak collisions: Gaussian process representation with correct asymptotic form, J. Chem. Phys. **150**, 064106 (2019).

[42] H. Sugisawa, T. Ida, and R. V. Krems, Gaussian process model of 51-dimensional potential energy surface for protonated imidazole dimer, J. Chem. Phys. **153**, 114101 (2020).

[43] J. Dai and R. V. Krems, Interpolation and extrapolation of global potential energy surfaces for polyatomic systems by gaussian processes with composite kernels, J. Chem. Theory Comput. **16**, 1386 (2020).

[44] H.-J. Werner, P. J. Knowles, G. Knizia, F. R. Manby, and M. Schütz, Molpro: A general-purpose quantum chemistry program package, WIREs Comput. Mol. Sci. **2**, 242 (2012).

[45] J. G. Hill and K. A. Peterson, Gaussian basis sets for use in correlated molecular calculations. XI. Pseudopotential-based and all-electron relativistic basis sets for alkali metal (K–Fr) and alkaline earth (Ca–Ra) elements, J. Chem. Phys. **147**, 244106 (2017).

[46] I. S. Lim, P. Schwerdtfeger, B. Metz, and H. Stoll, All-electron and relativistic pseudopotential studies for the group 1 element polarizabilities from k to element 119, J. Chem. Phys. **122**, 104103 (2005).

[47] R. A. Kendall, T. H. Dunning Jr, and R. J. Harrison, Electron affinities of the first-row atoms revisited: Systematic basis sets and wave functions, J. Chem. Phys. **96**, 6796 (1992).

[48] S. Hou and P. F. Bernath, Line list for the ground state of caf, J. Quant. Spectrosc. Radiat. Transfer **210**, 44 (2018).

[49] O. Allard, C. Samuelis, A. Pashov, H. Knöckel, and E. Tiemann, Experimental study of the Ca_2 $^1S + {}^1S$ asymptote, European Physical Journal D **26**, 155 (2003).

[50] K. P. Huber and G. Herzberg, *Molecular Spectra and Molecular Structure: IV. Constants of Diatomic Molecules* (Springer, Boston, 1979).

[51] W. J. Balfour and R. F. Whitlock, The visible absorption spectrum of diatomic calcium, Can. J. Phys. **53**, 472 (1975).

[52] E. Chen and W. Wentworth, Negative ion states of the halogens, J. Phys. Chem. **89**, 4099 (1985).

[53] J. Yang, Y. Hao, J. Li, C. Zhou, and Y. Mo, A combined zero electronic kinetic energy spectroscopy and ion-pair dissociation imaging study of the $F_2^+(X^2\pi_g)$ structure, J. Chem. Phys. **122**, 134308 (2005).

[54] L. Seijo, Z. Barandiarán, and S. Huzinaga, A binitio model potential study of the equilibrium geometry of alkaline earth dihalides: MX_2 (M= Mg, Ca, Sr, Ba; X= F, Cl, Br, I), J. Chem. Phys. **94**, 3762 (1991).

[55] M. Kaupp and P. v. R. Schleyer, The structural variations of monomeric alkaline earth MX_2 compounds (M= calcium, strontium, barium; X= Li, BeH, Bh, Ch3, Nh2, Oh, F). An *ab initio* pseudopotential study, J. Am. Chem. Soc. **114**, 491 (1992).

[56] J. B. Levy and M. Hargittai, Unusual dimer structures of the heavier alkaline earth dihalides: A density functional study, J. Phys. Chem. A **104**, 1950 (2000).

[57] L. von Szentpály, Hard bends soft: Bond angle and bending force constant predictions for dihalides, dihydrides, and dilithides of groups 2 and 12, J. Phys. Chem. A **106**, 11945 (2002).

[58] M. Kaupp, P. v. R. Schleyer, H. Stoll, and H. Preuss, The question of bending of the alkaline earth dihalides MX_2 (M= beryllium, magnesium, calcium, strontium, barium; X= fluorine, chlorine, bromine, iodine). An *ab initio* pseudopotential study, J. Am. Chem. Soc. **113**, 6012 (1991).

[59] J. Koput and A. Roszczak, CaF_2 as a quasilinear molecule: The vibrational- rotational energy levels predicted by *ab initio* quantum chemistry approach, J. Phys. Chem. A **108**, 9267 (2004).

[60] J. Cui and R. V. Krems, Efficient non-parametric fitting of potential energy surfaces for polyatomic molecules with gaussian processes, J. Phys. B **49**, 224001 (2016).

[61] C. K. Williams and C. E. Rasmussen, *Gaussian Processes for Machine Learning* (MIT, Cambridge, MA, 2006), Vol. 2.

[62] M. Stein, Large sample properties of simulations using latin hypercube sampling, Technometrics **29**, 143 (1987).

[63] D. Sardar, https://github.com/jila2021/singlet-CaF-CaF.git (2023).

[64] G. Henkelman, B. P. Uberuaga, and H. Jónsson, A climbing image nudged elastic band method for finding saddle points and minimum energy paths, J. Chem. Phys. **113**, 9901 (2000).